Direct proof of mesoscopic misfit in nanoscale islands by x-ray absorption spectroscopy

H. L. Meyerheim,[1,*] E. D. Crozier,[2] R. A. Gordon,[2] Q. F. Xiao,[2,†] K. Mohseni,[1] N. N. Negulyaev,[1] V. S. Stepanyuk,[1] and J. Kirschner[1]

[1]*Max-Planck-Institut für Mikrostrukturphysik, Weinberg 2, D-06120 Halle, Germany*

[2]*Department of Physics, Simon Fraser University Burnaby, V5A 1S6 British Columbia, Canada*

(Received 23 October 2011; revised manuscript received 21 December 2011; published 5 March 2012)

Polarization-dependent extended x-ray-absorption fine-structure measurements above the Co-K absorption edge were carried out to experimentally prove the theoretically predicted contraction of interatomic distances in nanoscale Co islands ($\oslash \approx 1$ nm) on Cu(001). Within the Co islands of thickness one monolayer (ML) which were deposited at 160 K substrate temperature, we find an in-plane Co-Co distance of 2.45 ± 0.02 Å, significantly shorter than in bulk Co (2.51 Å) and in close agreement with theoretical predictions. The effective in-plane coordination number $N^*_{\mathrm{Co}}(\|)$ is equal to 3.2 ± 0.5 and 5.0 ± 0.7 ($N^* = 6$ for an infinite island) for samples covered by 0.3 and 0.7 MLs of Co, respectively. The low value for the 0.3 ML sample is related to the finite island size and to about 20% of the intermixing between the adsorbate and substrate atoms. The experimental results are supported by molecular dynamics calculations.

DOI: 10.1103/PhysRevB.85.125405 PACS number(s): 61.05.cj, 61.46.Df, 68.43.−h

I. INTRODUCTION

Nanoscale objects on surfaces are intensely studied in solid-state physics due to their interesting physical and chemical properties, which are often considerably modified as compared to the bulk.[1–10] This is because a considerable fraction of the atoms experiences a reduced coordination involving broken bonds and significant structural rearrangement.[8–16] Despite the decisive importance of the atomic geometry for the physical properties of a nanostructure, its precise knowledge is comparatively scarce, since generally this geometry does not exhibit a well-defined long-range order.[17–20] This makes nanostructures difficult to analyze by classical diffraction methods. On the other hand, direct investigation by using scanning tunneling microscopy (STM) is often not possible due to the lack of sufficient lateral resolution.

For the study of the basic effects of spatial confinement, simple systems which can be prepared in an easy way are needed. In that respect, one of the most attractive systems is a submonolayer Co film deposited on a Cu surface, a model system for magnetic investigations over the last twenty years. The structural properties of cobalt films have been widely studied both experimentally and theoretically.[21–48] In particular, an ensemble of Co nanoislands grown on Cu(001) represents a system whose morphology is considered to be well understood.[44–47] STM experiments have indicated that, when adsorbed at temperatures far below 300 K to avoid surface diffusion of islands,[12] Co atoms on Cu(001) arrange in islands of about 1 nm in size, corresponding to about 16 atoms in the case of a square island.[47] Molecular-dynamics (MD) calculations have predicted[45,46] that depending on the island size the *average* interatomic distance is reduced by up to 5% with respect to the bulk lattice constant of Co (2.51 Å) due to the stronger bond experienced by the undercoordinated atoms at the edges of an island[49] and by the smoothing of the charge density as suggested by Smoluchowski.[50] This phenomenon is referred to as "mesoscopic misfit" (or "mesoscopic relaxations")[45,51] and can be seen as a general property of nanoislands.

The concept of the mesoscopic misfit has explained size-dependent atomic relaxations in nanoislands and enabled an understanding of the details of atomic diffusion on strained surfaces. For instance, it has been shown that mesoscopic relaxations strongly affect the shape of a substrate and nanoislands during homo-[52,53] and heteroepitaxy.[45] The relaxation can also change the details of atomic motion near the adislands[54] and on top of them.[46] The interplay between mesoscopic relaxations and activation barriers of interlayer mass transport at the edges of atomic-scale nanostructures has been revealed.[55] It has been found that mesoscopic relaxations in a substrate can induce surprisingly fast diffusion of small clusters,[43] which has a strong influence on the surface electronic structure of a nitrogen-covered metal substrate[56] and on the rates of chemical reactions on noble-metal surfaces.[57] The surface states over nanoscale islands are modified as the lateral size of an island changes, and this effect is also related to the size-dependent mesoscopic misfit.[29,58]

Despite some indirect experimental evidence from stress[59,60] and reflection high-energy electron-diffraction[61,62] experiments, the experimental verification of the concept of mesoscopic relaxations came only recently using surface x-ray diffraction (SXRD)[47,48] by analyzing the static disorder of the Co atoms relative to the fourfold hollow sites of the Cu(001) substrate. Although the SXRD analysis is in perfect agreement with theory,[47,48] it represents a rather indirect method for the quantification of the mesoscopic misfit, since the interatomic Co-Co distances were not directly determined. This calls for a more direct study of the internal geometry of nanoislands.

To this end, in this paper we have carried out an extended x-ray absorption fine-structure (EXAFS) study, which can directly reveal local structures around the absorbing atom.[63] Using polarization-dependent EXAFS spectra from the Co-K edge we show that Co-Co distances are contracted from 2.51 Å in the Co bulk to 2.45 Å within the islands of monolayer (ML) thickness, while the average effective coordination number (N^*) is sharply reduced from $N = 6^*$ in the case of an infinite monolayer to $N^* = 3.2 \pm 0.5$ and 5.0 ± 0.7 for a 0.3 and

0.7 ML film as a result of the finite island size. The remainder of the paper has the following structure. In Sec. II we describe the experimental procedure. The experimental results are presented in Sec. III. In Sec. IV we interpret the experimental data by comparison with theoretical calculations.

II. EXPERIMENT

X-ray-absorption fine-structure measurements were carried out at the Pacific Northwest Consortium X-Ray Science Division insertion device beamline at the Advanced Photon Source (APS), Argonne National Laboratory, using the MBE1 end station[64] equipped with standard surface analytical tools. Cobalt was deposited on the clean Cu(001) surface by electron-beam evaporation from a high-purity (99.999% metal) rod. The substrate temperature T was kept in the range between 155 and 170 K (designated henceforth as 160 K). The film coverage was calibrated by reflection high-energy electron-diffraction oscillations and by Auger-electron spectroscopy. Two different preparations were carried out, where 0.3 and 0.7 ML of Co were deposited at a rate of 0.4 ML per minute. Here and in the following we refer to one ML as 1.54×10^{15} atoms/cm^2, i.e., one adsorbate atom per substrate atom. From previous STM experiments[47,48] it is known that this procedure leads to one ML-thick nanoislands with a lateral size of about 1 nm.

The EXAFS measurements were carried out at the Co-K edge in the fluorescent yield (FY) mode using a seven-element solid-state Ge(Li) detector. Monochromatic x rays from a Si(111) double-crystal monochromator, with the APS ring operating in top-up mode, were incident on the substrate at approximately 2/3 of the critical angle ($\alpha_c \approx 0.4$ deg) for total reflection to avoid errors due to anomalous dispersion effects.[65] The substrates were oriented such that the electric-field vector of the linearly polarized x-ray beam was either perpendicular ($E \perp$, within α_c) or parallel ($E \parallel$) to the plane of the substrate with E oriented along the [100] direction. Small azimuthal adjustments (within 2 deg) were made to shift small Bragg peaks and more readily permit their removal. No azimuthal dependence of the EXAFS signal is expected due to the high ($p4mm$) plane group symmetry of the average adsorption structure. In addition, Co and Cu foils (EXAFS Materials, Inc.) were measured as reference samples in transmission mode at room temperature. The energy calibration of the monochromator was also monitored simultaneously with the film measurements using transmission of scattered radiation through the Co foil upstream of the beam defining slits.[66] The beam size was typically 50×1000 μm (unfocused undulator beam) with an incident intensity of approximately 2×10^{11} photons/sec as measured by a He-filled transmission ion chamber upstream of the sample after the beam defining slits.

III. RESULTS

A. Qualitative analysis

Four experiments were carried out on the film samples, in addition to the pure Cu and Co foils. A 0.3 ML film was studied in both perpendicular $E \perp$ and parallel $E \parallel$ orientations of the electric-field vector E at $T = 160$ K. A 0.7 ML film was prepared and data were collected in the $E \parallel$ geometry at 160 K for comparison. This film was also subsequently measured for $E \parallel$ at 295 K after an annealing at 370 K for 30 min.

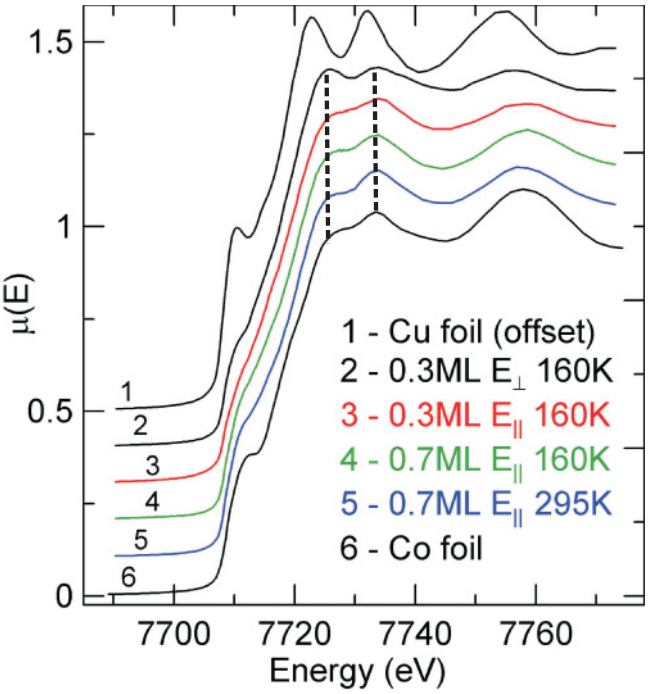

FIG. 1. (Color online) Comparison of near-edge absorption spectra labeled by nos. 1–6 and shifted vertically for clarity. Labels correspond to samples and experimental conditions as indicated in the inset. Dashed lines emphasize the maxima at 7725 and 7732 eV. Note that the Cu-K near-edge spectrum is shifted in energy to match the Co-K spectra.

The x-ray absorption near-edge structure (XANES) for each sample is shown in Fig. 1. The edge positions of the films exhibit no discernable shift from that of the Co foil. The three $E \parallel$ spectra are similar to that of the Co foil in having two features near 7725 and 7732 eV, with the 7725 eV feature noticeably lower in amplitude (see dashed lines in Fig. 1). This is in contrast to the 0.3 ML $E \perp$ spectrum, where the 7725 eV feature is comparable in amplitude to that at 7732 eV and reminiscent of the XANES of the Cu foil. This orientational anisotropy is not unexpected and can be interpreted as a qualitative indication that the $E \perp$ spectrum is dominated by Co-Cu correlation while in the case of the in-plane ($E \parallel$) spectra both Co-Co and Co-Cu correlations play a role.

EXAFS interference functions, χ(k), were extracted from the FY data using the program ATHENA[67,69] and are displayed in Fig. 2 as $k^2\chi(k)$ (where k is the wave vector of the emitted photoelectron). While Figs. 2(a) and 2(c) show the spectra for bulk Cu and Co, respectively, Fig. 2(b) compares four spectra collected for the four different samples, which are labelled according to the color code.

Differences between the spectra for $E \perp$ and $E \parallel$ are directly observable. Similar to the XANES spectra, the spectrum collected for the 0.3 ML sample in the $E \perp$ geometry bears similarities to that of the Cu foil, particularly in the shoulder-like features at 5.8 and 7.4 Å^{-1} [see arrows in Figs. 2(a) and 2(b)]. They are much less pronounced in the spectra

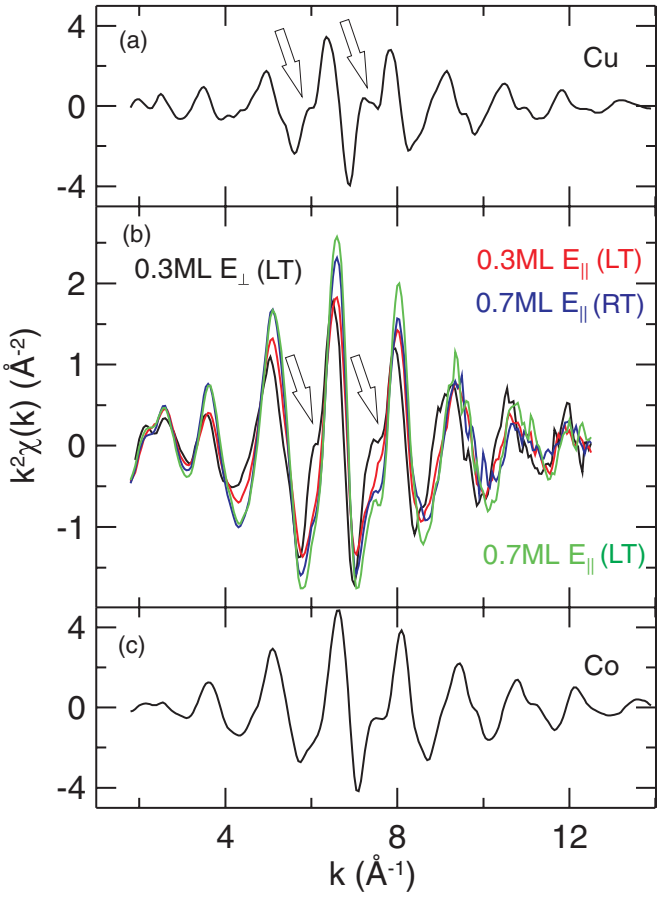

FIG. 2. (Color) (a) Comparison between interference functions $\chi(k) \times k^2$ obtained for bulk Cu (a) and Co (c) at room temperature as well as for different samples (b). Spectra are labeled according to color code: black, 0.3 ML $E \perp$ (LT); red, 0.3 ML $E \parallel$ (LT); blue, 0.7 ML $E \parallel$ (RT); and green, 0.7 ML $E \parallel$(LT), where LT and RT correspond to samples measured at 160 and 295 K, respectively. Arrows emphasize a spectral feature which is common to bulk Cu and the 0.3 ML $E \perp$ (LT) sample.

collected in $E \parallel$ geometry, especially for the 0.3 ML sample. As outlined below quantitatively, the polarization dependence of the EXAFS amplitude is related to polarization-dependent contributions of the first (consisting mainly of Co atoms) and second (consisting mainly of Cu atoms) shells around a Co atom on a surface. Here and in the following we refer to the first and second shell of atoms as the shell composed of Co atoms located at a distance of about 2.45 Å and the shell of Cu atoms located at a distance of about 2.54 Å, respectively (see below).

Fourier transforms (FTs) of the $k^2\chi$(k) spectra were calculated for each spectrum by using a 10% Gaussian window function in WinXAS code.[70] The k range used for the FT integration extends from $k_{\min} = 2.85$ Å^{-1} to $k_{\max} = 11.75$ Å^{-1} ($k_{\min}$ near 2.7 Å^{-1} for the reference foils). Figure 3 compares the FTs, in which the polarization dependence of the EXAFS spectra becomes directly evident.

Close inspection of the position of the first maximum indicates that the FT of the 0.3 ML $E \perp$ sample (black) is at a higher R value as compared to that of the 0.3 ML $E \parallel$ sample (red). Also, in both cases the FTs derived from the $E \parallel$ geometry have a contribution at the low-R side of the peak. As will be outlined quantitatively below, both observations are related to the presence of two shells (Cu and Co) instead of only one (Cu) in the case of the $E \perp$ geometry. Furthermore, the FT of the 0.7 ML sample exhibits a significantly larger absolute amplitude, pointing to an overall larger coordination number as compared to the 0.3 ML sample. The quantitative analysis is outlined in the following section.

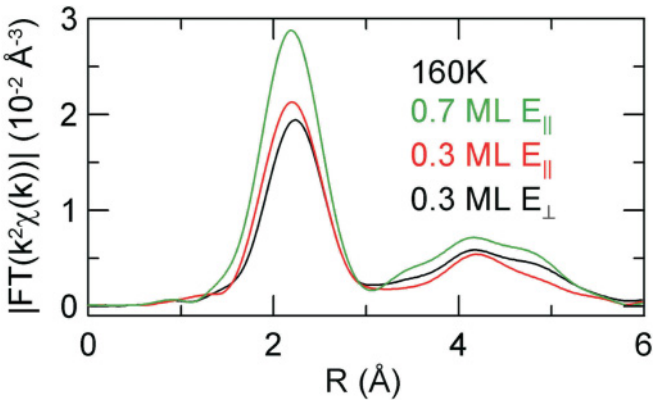

FIG. 3. (Color) Comparison between the Fourier transforms (FTs) derived for 0.7 ML $E \parallel$ (green), 0.3 ML $E \parallel$ (red), and 0.3 ML $E \perp$ (black).

B. Quantitative EXAFS analysis

Fitting of the EXAFS data was carried out using model amplitudes and phases generated by the FEFF7-program[71] implemented in the WinXAS program,[70] which allows the simultaneous fitting of both the k^2- and k^3-weighted spectra in order to reduce correlations between the structure parameters. The fits were carried out in real space (R space) over a typical range 1.6 to 2.7 Å in order to minimize any influence of multiple-scattering contributions and higher shells leaking into the first peak. For the analysis of the island structure a model calculation was carried out, in which the polarization dependence of the EXAFS amplitude was incorporated in the effective coordination number:

$$N_i^* = 3 \times \sum_{j=1}^{N} \cos^2(\alpha_{ij}), \tag{1}$$

in which α_{ij} represents the angle between electric-field vector E and the scattering path between the absorber i and the backscatterer j, where the summation extends over all atoms j of the shell. The effective coordination number N^* contributes to the EXAFS amplitude, which is part of the general EXAFS equation:

$$\chi(k) = \sum_i \frac{S_0^2 N_i^* F_i(k)}{k R_i^2} e^{(-2k^2\sigma_i^2)} e^{(-2R_i/\lambda_i)} \sin[2kR_i + \delta_i(k)], \tag{2}$$

with backscattering amplitudes $F_i(k)$, mean-free paths (λ_i), and phase shifts [$\delta_i(k)$] generated by FEFF. The parameter S_0^2 describes the effect the relaxation of the $(N-1)$ "passive" electrons has on the EXAFS amplitude after the photoelectron is emitted.[63,72] The remaining parameters, N^*_i (effective

TABLE I. Table of structural parameters. The meaning of the parameters are as follows: R, nearest-neighbor distance; N^*, effective coordination number; σ^2, mean-squared relative displacement amplitude; S_0^2, amplitude reduction factor; ΔE_0, shift of absorption edge; and Res, residual in percent.[73] Subscripts Co and Cu correspond to coordination shells composed of cobalt and copper atoms, respectively. The upper section compares experimental results for Cu and Co foils with bulk values. The center section lists the parameters for structural models used for the analysis. The lower section provides the fit results for the four different experiments. Numbers in square brackets represent parameters kept fixed. Symbols (‖) and (⊥) refer to experimental geometry with the electric-field vector parallel or perpendicular to the surface plane, respectively. Experiments were carried out at room temperature (RT) and 160 K (LT).

Sample	N^*_{Cu}	R_{Cu} (Å)	σ^2_{Cu} (Å^2)	N^*_{Co}	R_{Co} (Å)	σ^2_{Co} (Å^2)	S_0^2	ΔE_0 (eV)	Res
Cu crystal RT	12	2.556							
Cu foil RT	[12]	2.545(5)	0.0092(3)				0.98(3)	3.0(9)	0.48
Co crystal RT				12	2.507				
Co foil RT				[12]	2.493(5)	0.0066(3)	0.89(3)	6.1(1.0)	0.22
∞ layer RT	6(⊥)/3(‖)	2.553		6.0(‖)	2.554				
4 × 4 island RT	6(⊥)/3(‖)	2.553		4.5(‖)	2.554				
6 × 6 island RT	6(⊥)/3(‖)	2.553		5.0(‖)	2.554				
0.3 ML LT $E_\perp$	7.3(1.0)	2.544(10)	0.010(1)				[0.89]	3.9(1.0)	1.9
0.3 ML LT $E_\parallel$	[4.95]	[2.544]	0.008(1)	3.2(5)	2.45(2)	0.007(1)	[0.89]	3.0(1.0)/6.9(1.0)	1.4
0.7 ML LT $E_\parallel$	[4.95]	[2.544]	0.005(1)	5.0(7)	2.46(2)	0.007(1)	[0.89]	6.1(1.0)/7.3(1.0)	1.1
0.7 ML RT $E_\parallel$	[4.95]	[2.544]	0.009(1)	5.5(5)	2.46(2)	0.009(1)	[0.89]	4.9(1.0)/5.0(1.0)	1.0

coordination number), R_i (distance), and σ_i^2 (mean-square relative displacement), are available to be fit. In addition, a shift of the absorption edge energy ΔE_0 is used to correct for differences in energy levels between the sample and those taken from FEFF.

1. *Analysis of bulk Co and Cu*

As a first step we have carried out the analysis of the EXAFS spectra of the pure Cu and Co foils, and the results of this analysis are compared with the room temperature nearest-neighbor distances in Co and Cu (see upper section of Table I). We find that the first-shell distances are only slightly (≈0.01 Å) lower than the corresponding bulk values (2.545 ± 0.005 versus 2.556 Å) and (2.493 ± 0.005 versus 2.507 Å) for Cu and Co at room temperature, respectively.[68] The close agreement between our results and the known bulk values indicates that the phases $\delta_i(k)$ have proper values. More importantly, the analysis of the EXAFS amplitude allows us to derive the S_0^2 parameter, which will be used in the following for the fitting of the thin-film spectra. For the Cu and the Co foil we obtain $S_0^2 = 0.98 \pm 0.03$ and 0.89 ± 0.03, respectively. These data are summarized in the upper section of Table I.

2. *Analysis of Co/Cu(001) in E ⊥ geometry*

The next step of the analysis is the development of a structural model for the description of nanoscale Co islands on Cu(001). To this end we have used an undistorted Co island, with the atoms located in fourfold hollow sites of a Cu(001) surface closely following the structural model derived by low-energy electron diffraction for room temperature deposited Co on Cu(001).[74] It is schematically illustrated in Fig. 4 for an idealized 4 × 4 square island, representing an island with the lateral size of about 1 nm. The center section of Table I provides an overview of the structural parameters of the first two shells of a Co atom in an infinite, a 4 × 4, and a 6 × 6 island, the latter corresponding to a 1.5-nm-sized island.

In this idealized model, the distances to the Cu and the Co atoms (R_{Cu} and R_{Co}, respectively, see Fig. 4) are identical at 2.553 Å, in agreement with the model for a complete Co ML on Cu(001).[74] Owing to the mesoscopic misfit in nanoislands R_{Cu} and R_{Co} are expected to differ by a small amount. This is in contrast to previous EXAFS studies of Co films on Cu(001)[38] for coverages 3 ML and higher deposited at room temperature which indicated results opposite from the low-temperature, submonolayer work reported here. Heckmann *et al.*[38] found

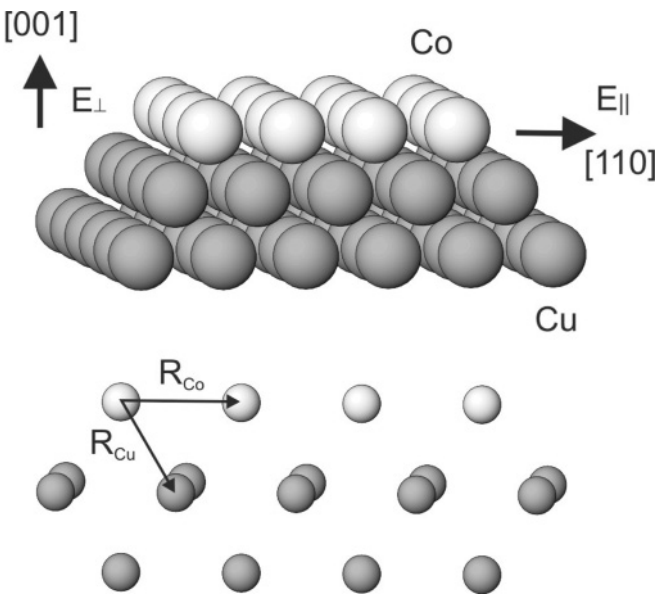

FIG. 4. Idealized model of the Co/Cu(001) island structure showing a 4 × 4 Co island (bright balls) and two Cu layers (dark balls). Co atoms are located in hollow sites.

that the films were lattice matching in-plane to the copper and contracted out of plane to a near-neighbor distance in Co metal.

It is not possible to separate the contribution of two closely situated shells, namely, (i) the Co shell, which is expected to be located at a distance of $R_{\mathrm{Co}} \approx 2.44-2.48$ Å, and (ii) the Cu shell, which is expected to be at a distance of $R_{\mathrm{Cu}} \approx 2.52-2.55$ Å.[45,52,75] The limited k range of the EXAFS spectra prevents the direct analysis of the shell separation on the basis of the beat pattern in the $\chi(k)$ function according to the relation[76,77] $\Delta R \approx \pi/(2\Delta k)$. For $\Delta R = 0.1$ Å the necessary k range is calculated to $\Delta k = 15.7$ Å^{-1}, which is considerably larger than $\Delta k \approx 9$ Å^{-1} available in this experiment.

Nevertheless, owing to the dipolelike distribution of the emitted photoelectron wave it is possible to disentangle the contributions from the two shells by taking advantage of the polarization dependence of the EXAFS amplitude. The polarization dependence is described by Eq. (1), which sets the relation between the effective coordination number and the angle α_{ij} between the E vector and the scattering path from an absorber to the j atoms in the ith shell. In the present case the effective coordination number of Cu atoms in the $E \perp$ geometry [$N^*_{\mathrm{Cu}}(\perp)$] is given by

$$N^*_{\mathrm{Cu}}(\perp) = 3 \times \sum_{j=1}^{4} \cos^2(\alpha_{2j}) = 6, \tag{3}$$

since if the E vector points into the sample, the angle α_{2j} is approximately equal to 45° for all four Cu atoms around the Co absorber. We have used the subscript "2" to emphasize that we are considering the second shell of neighbors. By contrast, for the $E \parallel$ geometry, $\alpha_{2j} = 60°$, leading to $N^*_{\mathrm{Cu}}(\parallel) = 3$.

The situation is different for the first shell, which is composed of Co atoms. The first shell does not contribute in the $E \perp$ geometry, since $\alpha_{1j} \approx 90°$, i.e., $N^*_{\mathrm{Co}}(\perp) = 0$. On the other hand, the Co shell *does* contribute in the $E \parallel$ geometry, and $N^*_{\mathrm{Co}}(\parallel)$ strongly depends on the island size.[78] In detail this is shown in Fig. 5, where $N^*_{\mathrm{Co}}(\parallel)$ is plotted versus the number of Co atoms assuming square islands for simplicity. For large island sizes, $N^*_{\mathrm{Co}}(\parallel)$ approaches $N^* = 6$, the effective coordination number in an infinite layer.

In this way, the Cu-shell contribution was isolated by using the EXAFS spectra taken in the $E \perp$ geometry. To this end the FT of the 0.3 ML sample was fitted to a single backscattering path. This procedure yields $R_{\mathrm{Cu}} = 2.544 \pm 0.010$ Å and $N^*_{\mathrm{Cu}}(\perp) = 7.3 \pm 1.0$. The derived distance R_{Cu} is consistent with the SXRD analysis in Ref. 48, where for several samples interplane Co-Cu distances in the range between 1.76 and 1.81 Å were found corresponding to R_{Cu} between 2.524 and 2.559 Å if the Co atom resides in the hollow site. Deeper vertical relaxations involving Cu-Cu spacings are not probed in our study. While R_{Cu} is in the expected range, the experimentally derived effective coordination number $N^*_{\mathrm{Cu}}(\perp) = 7.3 \pm 1.0$ is larger than the model value [$N^*_{\mathrm{Cu}}(\perp) = 6$] calculated for the $E \perp$ geometry. This apparent contradiction is attributed to intermixing, even at such low temperatures as 160 K (see Sec. IV for the explanation). An approximate quantitative estimate of the fraction f of embedded Co atoms is possible by taking into account that embedded Co atoms

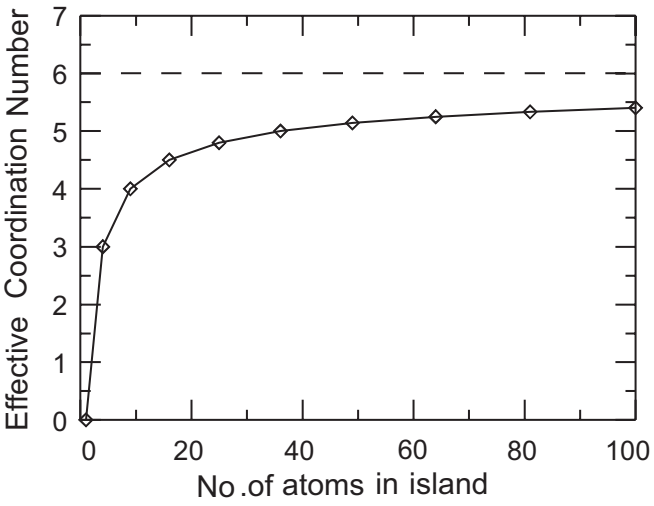

FIG. 5. Effective coordination number (N^*) of the Co shell vs number of Co atoms in a square nanoisland. The dashed line indicates the limit $N^* = 6$ for an infinite Co island.

experience a coordination of $N^*_{\mathrm{full}}(\perp) = 12$, leading to the following relation:

$$N^*_{\mathrm{fit}} \perp = f \times N^*_{\mathrm{full}} + (1 - f) N^*_{\mathrm{model}}, \tag{4}$$

from which we derive the fraction of embedded Co atoms as $f = 0.22 \pm 0.17$. The structure parameters derived for the $E_\perp$ geometry are summarized in the first row of the lower section of Table I.

3. *Analysis of Co/Cu(001) in E ∥ geometry*

In the next step $R_{\mathrm{Cu}}$and $N^*_{\mathrm{Cu}}(\perp)$ were kept fixed and the FTs derived from $E \parallel$ measurements were fit. By changing the experimental geometry from $E \perp$ to $E \parallel$, N^*_{Cu} must be corrected according to the relation $N^*_{\mathrm{Cu}}(\parallel) = 0.5 \times N^*_{\mathrm{Cu}}(\perp)$, which leads to $N^*_{\mathrm{Cu}}(\parallel) = 3.65 \pm 0.50$, if embedding of Co absorber atoms is neglected. However, embedding of Co into the Cu substrate also affects $N^*_{\mathrm{Cu}}(\parallel)$, because the embedded Co atoms are surrounded by a complete shell ($N^* = 6$) of Cu atoms at a distance of $R \approx 2.55$ Å. The fraction of embedded Co atoms f contributes by $6 \times f$ to $N^*_{\mathrm{Cu}}(\parallel)$ in addition to the contribution of $0.5 \times N^*_{\mathrm{Cu}}(\perp)$. Consequently, the in-plane effective coordination number $N^*_{\mathrm{Cu}}(\parallel)$ can be written in terms of the out-of-plane effective coordination number $N^*_{\mathrm{Cu}}(\perp)$:

$$N^*_{\mathrm{Cu}}(\parallel) = 1.5 \times N^*_{\mathrm{Cu}}(\perp) - 6. \tag{5}$$

This constraint is applied to fit the $E \parallel$ FTs. In the present case $N^*_{\mathrm{Cu}}(\perp) = 7.3$, which leads to $N^*_{\mathrm{Cu}}(\parallel) = 4.95$. The lower part of Table I summarizes the fit results for all experiments carried out in the $E \parallel$ geometry. There are two remarkable results. First, there is a significant reduction of R_{Co} from 2.51 Å in bulk Co to 2.45 Å in the island. We also find a significant reduction in $N^*_{\mathrm{Co}}(\parallel)$ to values in the 3.2 to 5.5 range for the 0.3- and 0.7 ML sample, respectively [$N^*_{\mathrm{Co}}(\parallel) = 6$ for an infinitely large island].

Very high-quality fits were achieved in general. The fit quality is quantified by the unweighted residuum (see Table I and Ref. 73), which lies in the 1% range for all data. One example is shown in Fig. 6, in which the magnitude and

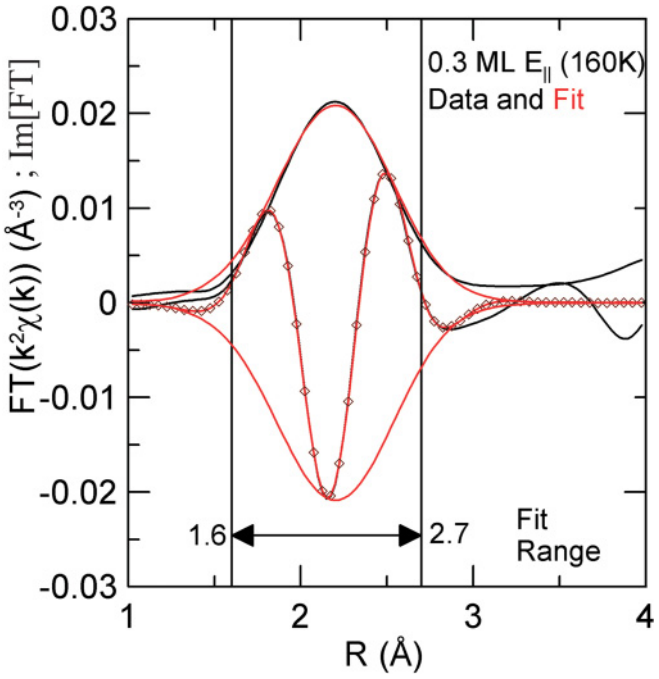

FIG. 6. (Color online) Comparison of FTs between data and fit for 0.3 ML $E \parallel$ (160 K). The k^2-weighted FTs were taken over the same k-space range (2.85–11.75 Å^{-1}) with a 10% Gaussian window function. Black and red curves represent experimental and calculated |FT| and Im(FT), respectively. The calculated Im(FT) is emphasized by the dotted red curve.

the imaginary part [Im(FT)] of the experimentally derived FT (black curves) is compared with the calculated ones [red curves, with symbols for Im(FT)]. Within the selected range between 1.6 and 2.7 Å experimental and calculated curves almost perfectly overlap.

Uncertainties for the structural parameters were estimated by carrying out extensive raster calculations, one of which is shown in Fig. 7 for the 0.3 ML sample. Here, the residuum

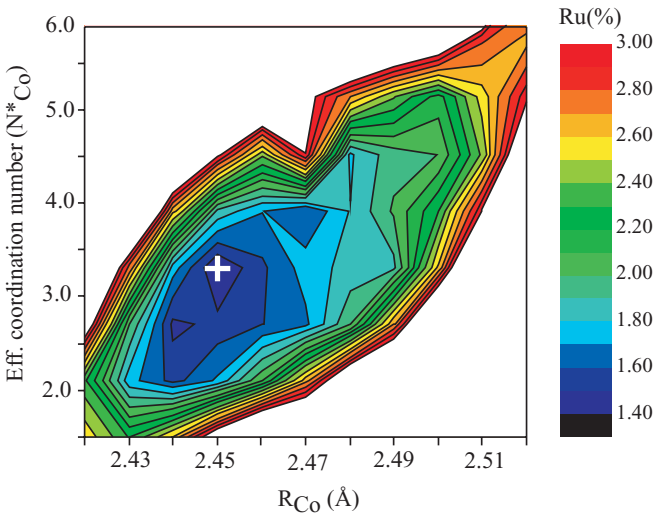

FIG. 7. (Color) Contour plot of $N^*_{\mathrm{Co}}(\parallel)$ and R_{Co} vs Ru for the 0.3 ML sample. The cross marks the minimum. The color code for the residual Ru is shown on the right.

of the fit (Ru) (Ref. 73) is plotted versus $N^*_{\mathrm{Co}}(\parallel)$ and R_{Co}. The cross marks the minimum. Allowance for an increase of Ru in the 10–20% range as indicated by the bar is used to estimate the uncertainty, which is about 0.02 Å for R_{Co} and 0.5 for $N^*_{\mathrm{Co}}(\parallel)$. It should be emphasized that the uncertainties derived in this way include correlations with the parameters σ and ΔE_0 which were allowed to vary. Table I lists the best fit parameters and the Ru for all three samples.

IV. INTERPRETATION OF THE RESULTS

The EXAFS analysis allows detailed insights into the structure of the Co islands grown on Cu(001) at different coverages. The first important result of our study relates to the average Co-Co distance. The analysis shows that for the 0.3 ML sample the average interatomic distance within the islands equals to 2.45 ± 0.02 Å, while for a 0.7 ML film the corresponding value is 2.46 ± 0.02 Å.

For direct comparison we have carried out a theoretical analysis of the interatomic Co-Co distances in ensembles of Co nanoislands grown on a Cu(001) surface after the deposition of 0.3 and 0.7 ML of Co atoms at 160 K. Since the direct *ab initio* analysis of nanoislands containing about 50 atoms in fully relaxed geometry is hardly possible, in the present case we have used large-scale atomic simulations by means of the MD method.[79] Our theoretical study finds that at the given experimental conditions the ensemble averaged Co-Co distance is equal to 2.43 and 2.45 Å for the 0.3 and the 0.7 ML sample, respectively. These values are in good agreement with those obtained from the current EXAFS analysis. This issue represents a remarkable result in that it is a direct proof of the mesoscopic misfit in nanoscale monolayers using a structure analysis method.

The second important result is the small effective coordination number $N^*_{\mathrm{Co}}(\parallel) = 3.2 \pm 0.5$ for a 0.3 ML Co film on Cu(001). According to the square island model (see Fig. 5) an effective coordination number of $N^*_{\mathrm{Co}}(\parallel) = 3.2 \pm 0.5$ is related to an island size of a few atoms only. Such a small island size has not been observed in previous STM experiments,[47,48] which indicate a typical island size of about 1.0 and in some cases even 1.5 nm. Within the square island model these sizes correspond to 4×4 and 6×6 islands, respectively. The (apparent) disagreement between (STM) observed and estimated island size might have several reasons: At first, it should be noted that the island size might be overestimated in STM experiments due to the tip island convolution (see below). Second, from the independent analysis of the coordination number derived from the experiments carried out in the $E \perp$ geometry, there is evidence for a 10–20% of alloying of Co atoms (see Sec. III.B.2), which should also lead to a reduction of $N^*_{\mathrm{Co}}(\parallel)$.

In order to provide a quantitative explanation we discuss a simple model. Figure 8 shows an island consisting of $N = 18$ atoms corresponding to an island size of 1.3 nm along the [110] direction. Bright and dark spheres represent substrate (Cu) and adlayer (Co) atoms, respectively. An intermixing fraction of $f = 0.2$ roughly corresponds to four atoms, which are exchanged. The exchanged Cu atoms which are now embedded into the island are shown darker and are labeled accordingly. In the in-plane geometry, the electric-field vector was oriented along the [110] direction and the effective coordination number

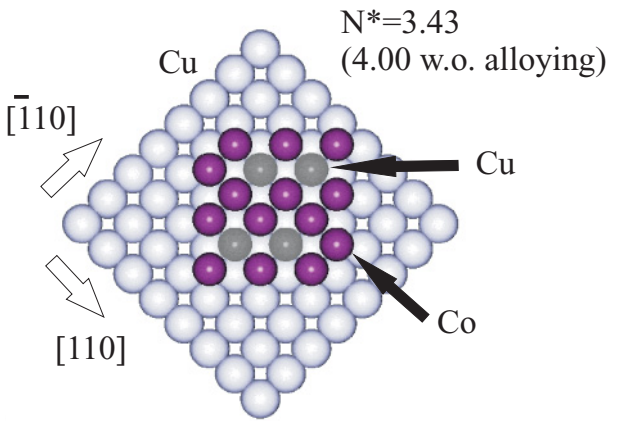

FIG. 8. (Color online) Schematic view of an 18-atom island. Cu substrate atoms are represented as bright spheres. Co-adlayer atoms (dark) and exchanged Cu atoms inside the Co island (black) are labeled.

of the Co atoms within the island can be directly calculated. For simplicity we have assumed an isometric island shape, but the detailed shape of the island does not strongly affect the (average) coordination number as long as no extremely anisotropic (e.g., dendritic) shape is assumed.

For the nonalloyed island (i.e., an island which is composed of Co atoms only) the effective coordination number equals $N^*_{\mathrm{Co}}(\|) = 4.00$. We have also considered the island size distribution as shown in Figs. 3 and 5 of Refs. 48. For the largest and smallest islands we find values in the range between $N^*_{\mathrm{Co}}(\|) = 3.81$ and 4.80. Thus, the *isolated* island shown in Fig. 8 can be viewed as representative for the 0.3 ML sample. In this case allowing for a 20% alloying significantly reduces the (average) coordination number from $N^*_{\mathrm{Co}}(\|) = 4.00$ to 3.43, in quite good agreement with experiment. Here, it is assumed that the exchanged Cu atoms (black spheres) reside inside the island and not at the rim, in this way replacing only those Co atoms which experience a high coordination number $N^*_{\mathrm{Co}}(\|) = 6$. It should be noted that the presence of vacancies inside an island would be very effective in reducing $N^*_{\mathrm{Co}}(\|)$ but appears as rather unlikely because of the considerable mobility of the adatoms at the surface, even at 160 K.

As noted previously, owing to the tip island convolution and depending on the tip conditions the (apparent) size of the islands might be larger than their "true" one by several tens of a percent. This possibility leads to the agreement between the experimental value of $N^*_{\mathrm{Co}}(\|)$ and that calculated for a (smaller) model island and would not necessarily require the assumption of a 20% alloying. Nevertheless, the independent experimental evidence of a ≈20% intermixing (see Sec. III.B.2) is supported by theory: The theoretical studies suggest that, though the probability of the embedding of the deposited Co atoms into the topmost substrate layer is almost zero at very low coverage (≪0.1 ML), alloying is possible as the Co coverage increases. Alloying is possible even at the low temperature (160 K) at which the deposition and the experiments were carried out.

In order to understand the origin of the alloying mechanism, one has to take into account that the kinetics of an adatom on a surface is determined by the relation between two parameters:

TABLE II. Energy difference $(E_I - E_D)$ between the activation barrier for the embedding of a Co atom into the topmost Cu(001) layer E_I and the activation barrier for the hopping of such an atom on a surface E_D as a function of the tetragonal tensile strain. Also shown is the energy gain E_g caused by the incorporation of a Co adatom into the topmost substrate layer as a function of the tetragonal tensile strain. The data are obtained by means of MD simulations.[79]

Strain (%)	0	1	2	3
$E_I - E_D$ (eV)	0.22	0.08	−0.05	−0.17
E_g (eV)	0.49	0.48	0.46	0.44

(i) the hopping diffusion barrier E_D and (ii) the diffusion barrier for the intermixing E_I. If the incorporation of an adsorbate into the surface layer is energetically favorable, the relative frequency of these two events is defined by means of the ratio $\nu_{\mathrm{rel}} = \nu_I/\nu_D = \exp[-(E_I - E_D)/k_B T]$, where k_B is the Boltzmann constant and T is the temperature of the substrate. For $\nu_{\mathrm{rel}} \ll 1$ embedding is kinetically not possible. If the surface diffusion length of the deposited atoms is large enough, the atoms attach to the existing island and thus do not incorporate into the substrate. By contrast, for $\nu_{\mathrm{rel}} \gg 1$, the incorporation is kinetically possible and the atoms embed. If the coverage of deposited atoms is small enough and there are no islands, the energy difference $(E_I - E_D) = 0.22$ eV, and thus $\nu_{\mathrm{rel}} \sim 10^{-7}$, and no embedding of Co atoms is possible.[79]

However, if the fraction of the deposited Co is high enough, and the strain caused by the mesoscopic misfit arises in the substrate around the islands,[45,52,75] alloying is possible. It is known that even small values of surface strain could promote dramatic modifications of the values of the activation barriers E_D and E_I: tensile strain increases the activation barrier for the hopping diffusion and decreases the activation barrier for the embedding (for compressive strain the tendency is opposite).[84,85] In the examined case, Co/Cu(001), the substrate below the Co islands is under compressive strain, while it is under tensile strain around the islands.[45,75] It is remarkable that the magnitude of the tensile strain around the islands reaches 2%.[45,75] Table II demonstrates how the energy difference $(E_I - E_D)$ depends on the value of the tetragonal tensile strain. Since the sign of the energy difference $(E_I - E_D)$ is modified, as the tetragonal strain reaches ≈1.5%, the surface diffusion is not kinetically possible anymore, and the incorporation of Co atoms takes place (it is important that for all considered values of the tensile strain, the embedding of Co into the topmost substrate layer is energetically favorable). As a result, our theoretical analysis suggests that, while at the early deposition stages incorporation of Co into the topmost Cu(001) substrate layer is not possible, it plays an important role after Co islands are formed.

The third result of our EXAFS studies is that there is a distinct dependence of $N^*_{\mathrm{Co}}(\|)$ on the Co coverage. For the as-deposited (160 K) 0.7 ML sample we find $N^*_{\mathrm{Co}}(\|) = 5.0 \pm 0.7$, which is considerably larger than the effective coordination number of $N^*_{\mathrm{Co}}(\|) = 3.2 \pm 0.5$, determined for the 0.3 ML sample. We attribute this effect not only to an increase of the island size with increasing coverage but also to the coalescence of the islands as observed in STM.[47] In agreement with this model, after sample annealing a further increase of $N^*_{\mathrm{Co}}(\|) =$

5.5 ± 0.5 is observed, corresponding to an island size larger than 100 atoms.

V. SUMMARY

We have carried out an EXAFS study of the local structure of nanoscale monolayer-thick Co islands grown on a Cu(001) surface at 160 K. This system represents the classical system for the verification of the concept of mesoscopic misfit. Using the polarization dependence of the effective coordination number, it is possible to separate the contributions of the two closely neighboring shells next to a Co atom on a surface, namely, Co at a distance of $R_{\mathrm{Co}} = 2.45 \pm 0.02$ Å and Cu at a distance of $R_{\mathrm{Cu}} = 2.54 \pm 0.01$ Å. We have resolved the contraction of the interatomic Co-Co distance from 2.51 Å in bulk Co [2.56 Å in the fourfold hollow site on Cu(001)] to 2.45 Å. The last result is in agreement with theoretical predictions for Co islands in the 20–30-atom size range. The strong reduction of the average effective coordination number $[N^*_{\mathrm{Co}}(\|)]$ from 6 for an infinite island to about 3.2 ± 0.05 in the 0.3 ML sample is related to both the finite island size and to a 20% alloying, where Co and Cu atoms are exchanged. In the case of the 0.7 ML sample, $N^*_{\mathrm{Co}}(\|)$ reaches values in the range from 5.0 to 5.5 for the as-deposited and annealed sample, which is attributed to island coalescence. These values are still less than $N^* = 6$ for an infinitely large island, due to the pronounced number of the undercoordinated atoms. The experimental results are supported by *ab initio* and molecular-dynamics calculations. Even at a temperature of 160 K, intermixing is kinetically possible due to the reduction of the activation barrier by strain resulting from the mesoscopic misfit.

ACKNOWLEDGMENTS

We thank M. Balasubramanian for insightful discussions. Pacific Northwest Consortium X-Ray Science Division facilities at the Advanced Photon Source and research at these facilities are supported by the US Department of Energy (DOE), Basic Energy Sciences, a Major Resources Support grant from the Natural Sciences and Engineering Research Council of Canada, the University of Washington, Simon Fraser University, and the Advanced Photon Source. Use of the Advanced Photon Source, an Office of Science User Facility operated for the US DOE Office of Science by Argonne National Laboratory, was supported by the US DOE under Contract No. DE-AC02-06CH11357.

*hmeyerhm@mpi-halle.mpg.de

†Present address: Canadian Light Source, Saskatoon, S7N0X4 Saskatchewan, Canada.

[1] T. L. Einstein and J. R. Schrieffer, Phys. Rev. B **7**, 3629 (1973).

[2] H. Brune, M. Giovannini, K. Bromann, and K. Kern, Nature (London) **394**, 451 (1998).

[3] V. A. Shchukin and D. Bimberg, Rev. Mod. Phys. **71**, 1125 (1999).

[4] J. V. Barth, G. C. Costantini, and K. Kern, Nature (London) **437**, 671 (2005).

[5] Y. Pennec, W. Auwärter, A. Schiffrin, A. Weber-Bargioni, A. Riemann, and J. V. Barth, Nature Nanotech. **2**, 99 (2007).

[6] N. N. Negulyaev, V. S. Stepanyuk, L. Niebergall, P. Bruno, M. Pivetta, M. Ternes, F. Patthey, and W.-D. Schneider, Phys. Rev. Lett. **102**, 246102 (2009).

[7] O. U. Uche, D. Perez, A. F. Voter, and J. C. Hamilton, Phys. Rev. Lett. **103**, 046101 (2009).

[8] A. Enders, R. Skomski, and J. Honolka, J. Phys. Condens. Matter **22**, 433001 (2010).

[9] Z. Cheng, J. Wyrick, M. Luo, D. Sun, D. Kim, Y. Zhu, W. Lu, K. Kim, T. L. Einstein, and L. Bartels, Phys. Rev. Lett. **105**, 066104 (2010).

[10] K. Kim and T. L. Einstein, Phys. Rev. B **83**, 245414 (2011).

[11] R. A. Miron and K. A. Fichthorn, Phys. Rev. Lett. **93**, 128301 (2004).

[12] C.-G. Duan, J. P. Velev, R. F. Sabirianov, Z. Zhu, J. Chu, S. S. Jaswal, and E. Y. Tsymbal, Phys. Rev. Lett. **101**, 137201 (2008).

[13] Y. Nahas, V. Repain, C. Chacon, Y. Girard, J. Lagoute, G. Rodary, J. Klein, S. Rousset, H. Bulou, and C. Goyhenex, Phys. Rev. Lett. **103**, 067202 (2009).

[14] N. N. Negulyaev, V. S. Stepanyuk, L. Niebergall, P. Bruno, W. Auwärter, Y. Pennec, G. Jahnz, and J. V. Barth, Phys. Rev. B **79**, 195411 (2009).

[15] J. D. Howe, P. Bhopale, Y. Tiwary, and K. A. Fichthorn, Phys. Rev. B **81**, 121410 (2010).

[16] Y. Sun, J. D. Burton, and E. Y. Tsymbal, Phys. Rev. B **81**, 064413 (2010).

[17] L.P. Nielsen, F. Besenbacher, I. Stensgaard, E. Lægsgaard, C. Engdahl, P. Stoltze, K. W. Jacobsen, and J. K. Nørskov, Phys. Rev. Lett. **71**, 754 (1993).

[18] P. Poulopoulos, P. J. Jensen, A. Ney, J. Lindner, and K. Baberschke, Phys. Rev. B **65**, 064431 (2002).

[19] H. L. Meyerheim, D. Sander, N. N. Negulyaev, V. S. Stepanyuk, R. Popescu, I. Popa, and J. Kirschner, Phys. Rev. Lett. **100**, 146101 (2008).

[20] J. Honolka, T. Y. Lee, K. Kuhnke, A. Enders, R. Skomski, S. Bornemann, S. Mankovsky, J. Minar, J. Staunton, H. Ebert, M. Hessler, K. Fauth, G. Schütz, A. Buchsbaum, M. Schmid, P. Varga, and K. Kern, Phys. Rev. Lett. **102**, 067207 (2009).

[21] J. de la Figuera, J. E. Prieto, C. Ocal, and R. Miranda, Phys. Rev. B **47**, 13043 (1993).

[22] M. Ø. Pedersen, A. Bönicke, E. Lægsgaard, I. Stensgaard, A. Ruban, J. K. Nørskov, and F. Besenbacher, Surf. Sci. **387**, 86 (1997).

[23] A. L. Vázquez de Parga, F. J. García-Vidal, and R. Miranda, Phys. Rev. Lett. **85**, 4365 (2000).

[24] J. E. Prieto, J. de la Figuera, and R. Miranda, Phys. Rev. B **62**, 2126 (2000).

[25] J. Osterwalder, T. Greber, E. Wetli, J. Wider, and H. J. Neff, Prog. Surf. Sci. **64**, 65 (2000).

[26] L. Diekhöner, M. A. Schneider, A. N. Baranov, V. S. Stepanyuk, P. Bruno, and K. Kern, Phys. Rev. Lett. **90**, 236801 (2003).

[27] O. Pietzsch, S. Okatov, A. Kubetzka, M. Bode, S. Heinze, A. Lichtenstein, and R. Wiesendanger, Phys. Rev. Lett. **96**, 237203 (2006).

[28] H. W. Chang, F. T. Yuan, Y. D. Yao, W. Y. Cheng, W. B. Su, C. S. Chang, C. W. Lee, and W. C. Cheng, J. Appl. Phys. **100**, 084304 (2006).

[29] M. V. Rastei, B. Heinrich, L. Limot, P. A. Ignatiev, V. S. Stepanyuk, P. Bruno, and J. P. Bucher, Phys. Rev. Lett. **99**, 246102 (2007).

[30] N. N. Negulyaev, V. S. Stepanyuk, P. Bruno, L. Diekhöner, P. Wahl, and K. Kern, Phys. Rev. B **77**, 125437 (2008).

[31] P.-J. Hsu, C.-I. Lu, S.-W. Chen, W.-J. Hsueh, Y.-H. Chu, C.-H. Hsu, C. J. Butler, and M.-T. Lin, Appl. Phys. Lett. **96**, 142515 (2010).

[32] J. Bork, J. Onsgaard, and L. Diekhöner, J. Phys. Condens. Matter **22**, 135005 (2010).

[33] H. Oka, P. A. Ignatiev, S. Wedekind, G. Rodary, L. Niebergall, V. S. Stepanyuk, D. Sander, and J. Kirschner, Science **327**, 843 (2010).

[34] D. Böttcher, A. Ernst, and J. Henk, J. Phys. Condens. Matter **23**, 296003 (2011).

[35] S. Hope, M. Tselepi, E. Gu, T. M. Parker, and J. A. C. Bland, J. Appl. Phys. **85**, 6094 (1999).

[36] S. M. York and F. M. Leibsle, Phys. Rev. B **64**, 033411 (2001).

[37] O. V. Stepanyuk, N. N. Negulyaev, A. M. Saletsky, and W. Hergert, Phys. Rev. B **78**, 113406 (2008).

[38] O. Heckmann, H. Mangan, P. Le Fevre, D. Chandesris, and J. J. Rehr, Surf. Sci. **312**, 62 (1994).

[39] P. Le Fevre, H. Mangan, D. Chandesris, and J. J. Rehr, Surf. Sci. **352–354**, 923 (1996).

[40] F. Nouvertné, U. May, M. Bamming, A. Rampe, U. Korte, G. Güntherodt, R. Pentcheva, and M. Scheffler, Phys. Rev. B **60**, 14382 (1999).

[41] R. Pentcheva and M. Scheffler, Phys. Rev. B **65**, 155418 (2002).

[42] R. Pentcheva, K. A. Fichthorn, M. Scheffler, T. Bernhard, R. Pfandzelter, and H. Winter, Phys. Rev. Lett. **90**, 076101 (2003).

[43] R. A. Miron and K. A. Fichthorn, Phys. Rev. B **72**, 035415 (2005).

[44] N. A. Levanov, V. S. Stepanyuk, W. Hergert, D. I. Bazhanov, P. H. Dederichs, A. A. Katsnelson, and C. Massobrio, Phys. Rev. B **61**, 2230 (2000).

[45] V. S. Stepanyuk, D. I. Bazhanov, A. N. Baranov, W. Hergert, P. H. Dederichs, and J. Kirschner, Phys. Rev. B **62**, 15398 (2000).

[46] V. S. Stepanyuk, D. I. Bazhanov, W. Hergert, and J. Kirschner, Phys. Rev. B **63**, 153406 (2001).

[47] O. Mironets, H. L. Meyerheim, C. Tusche, V. S. Stepanyuk, E. Soyka, P. Zschack, H. Hong, N. Jeutter, R. Felici, and J. Kirschner, Phys. Rev. Lett. **100**, 096103 (2008).

[48] O. Mironets, H. L. Meyerheim, C. Tusche, V. S. Stepanyuk, E. Soyka, H. Hong, P. Zschack, N. Jeutter, R. Felici, and J. Kirschner, Phys. Rev. B **79**, 035406 (2009).

[49] L. Pauling, J. Am. Chem. Soc. **69**, 542 (1947).

[50] R. Smoluchowski, Phys. Rev. **60**, 661 (1941).

[51] R. Kern and P. Müller, Surf. Sci. **392**, 103 (1997).

[52] O. V. Lysenko, V. S. Stepanyuk, W. Hergert, and J. Kirschner, Phys. Rev. Lett. **89**, 126102 (2002).

[53] R. Dana and Y. Manassen, Europhys. Lett. **79**, 16001 (2007).

[54] D.V. Tsivlin, V. S. Stepanyuk, W. Hergert, and J. Kirschner, Phys. Rev. B **68**, 205411 (2003).

[55] N. N. Negulyaev, V. S. Stepanyuk, W. Hergert, P. Bruno, and J. Kirschner, Phys. Rev. B **77**, 085430 (2008).

[56] D. Sekiba, K. Nakatsuji, Y. Yoshimoto, and F. Komori, Phys. Rev. Lett. **94**, 016808 (2005).

[57] D. Sekiba, Y. Yoshimoto, K. Nakatsuji, Y. Takagi, T. Iimori, S. Doi, and F. Komori, Phys. Rev. B **75**, 115404 (2007).

[58] F. Donati, G. Fratesi, M. Passoni, C. S. Casari, A. Mairov, C. E. Bottani, M. I. Trioni, and A. Li Bassi, Phys. Rev. B **83**, 153404 (2011).

[59] A. Grossmann, W. Erley, J. B. Hannon, and H. Ibach, Phys. Rev. Lett. **77**, 127 (1996).

[60] D. Sander, S. Ouazi, V. S. Stepanyuk, D. I. Bazhanov, and J. Kirschner, Surf. Sci. **512**, 281 (2002).

[61] J. Fassbender, U. May, B. Schirmer, R. M. Jungblut, B. Hillebrands, and G. Guntherodt, Phys. Rev. Lett. **75**, 4476 (1995).

[62] P. Turban, L. Hennet, and S. Andrieu, Surf. Sci. **446**, 241 (2000).

[63] J. Stöhr, in *X-Ray Absorption Spectroscopy: Applications, Techniques of EXAFS, SEXAFS, and XANES*, edited by D. C. Koningsberger and R. Prins (Wiley, New York, 1988), Chap. 10.

[64] R. A. Gordon, E. D. Crozier, D.-T. Jiang, J. Shoults, W. Barg, and P. S. Budnik, AIP Conf. Proc. **882**, 887 (2007).

[65] D. T. Jiang and E. D. Crozier, Can. J. Phys. **76**, 621 (1998).

[66] J. O. Cross and A. L. Frenkel, Rev. Sci. Instrum. **70**, 38 (1999).

[67] B. Ravel and M. Newville, J. Synchrotron Radiat. **12**, 537 (2005).

[68] H. W. King, in *Handbook of Chemistry and Physics*, edited by D. R. Lide (CRC, Boca Raton, 1994).

[69] M. Newville, J. Synchrotron Radiat. **8**, 322 (2001).

[70] T. Ressler, J. Synchrotron Radiat. **5**, 118 (1998).

[71] S. I. Zabinsky, J. J. Rehr, A. Ankudinov, R. C. Albers, and M. J. Eller, Phys. Rev. B **52**, 2995 (1995).

[72] E. A. Stern, B. A. Bunker, and S. M. Heald, Phys. Rev. B **21**, 5521 (1980).

[73] The unweighted residuum (Ru) is defined by $\mathrm{Ru} = \sum(Y\mathrm{obs} - Y\mathrm{calc})/\sum(Y\mathrm{obs})$, where Yobs and Ycalc are the experimental and calculated magnitudes of the peak selected in the FT of the $\chi(k)$ spectrum and the summation extends over all points in the window used to filter the peak.

[74] J. R. Cerdá, P. L. de Andres, A. Cebollada, R. Miranda, E. Navas, P. Schuster, C. M. Schneider, and J. Kirschner, J. Phys. Condens. Matter **5**, 2055 (1993).

[75] V. S. Stepanyuk, D. V. Tsivline, D. I. Bazhanov, W. Hergert, and A. A. Katsnelson, Phys. Rev. B **63**, 235406 (2001).

[76] K. R. Bauchspiess, Ph.D. thesis, Simon Fraser University, 1990.

[77] E. A. Stern, J. Synchrotron Radiat. **8**, 49 (2001).

[78] E. D. Crozier, A. J. Seary, M. K. McManus, and D. T. Jiang, J. Phys. IV France **7**, C2-251 (1997).

[79] The exploited interatomic potentials for the system of Cu and Co atoms (Cu-Cu, Cu-Co, and Co-Co) are formulated in the second moment approximation of the tight-binding approach. [80,81] The first-principle Korringa-Kohn-Rostocker Green's-function method [82,83] is used to create an *ab initio* data pool for the fitting of parameters of these potentials.[44] The parameters of the potentials are given in Ref. 30. Such potentials (i) reproduce the bulk properties of Cu and Co crystals, (ii) reproduce the *ab initio* calculated properties of supported and embedded Co clusters,[30] and (iii) properly describe the major details of the growth of thin Co films on different types of Cu surfaces: (111),[30] (110),[37] and (001).[44] The MD simulations are performed with a finite slab of ten layers, and three bottom layers are kept fixed. Each layer contains 676 atoms, and periodic boundary conditions are applied in the surface plane.

[80] V. Rosato, B. Guillope, and B. Legrand, Philos. Mag. A **59**, 321 (1989).

[81] F. Cleri and V. Rosato, Phys. Rev. B **48**, 22 (1993).

[82] K. Wildberger, V. S. Stepanyuk, P. Lang, R. Zeller, and P. H. Dederichs, Phys. Rev. Lett. **75**, 509 (1995).

[83] V. S. Stepanyuk, A. N. Baranov, D. V. Tsivlin, W. Hergert, P. Bruno, N. Knorr, M. A. Schneider, and K. Kern, Phys. Rev. B **68**, 205410 (2003).

[84] B. D. Yu and M. Scheffler, Phys. Rev. B **56**, R15569 (1997).

[85] W. Xiao, P. A. Greaney, and D. C. Chrzan, Phys. Rev. Lett. **90**, 156102 (2003).